Functional divergence caused by mutations in an energetic hotspot in ERK2

Clinton A. Taylor IV[a], Kevin W. Cormier[a,1], Shannon E. Keenan[b], Svetlana Earnest[a], Steve Stippec[a], Chonlarat Wichaidit[a], Yu-Chi Juang[a,2], Junmei Wang[c,3], Stanislav Y. Shvartsman[b], Elizabeth J. Goldsmith[c], and Melanie H. Cobb[a,4]

[a]Department of Pharmacology, UT Southwestern Medical Center, Dallas, TX 75390; [b]Department of Chemical and Biological Engineering, Lewis-Sigler Institute for Integrative Genomics, Princeton University, Princeton, NJ 08544; and [c]Department of Biophysics, UT Southwestern Medical Center, Dallas, TX 75390

Contributed by Melanie H. Cobb, June 7, 2019 (sent for review April 1, 2019; reviewed by Anton M. Bennett and Paul S. Shapiro)

The most frequent extracellular signal-regulated kinase 2 (ERK2) mutation occurring in cancers is E322K (E-K). ERK2 E-K reverses a buried charge in the ERK2 common docking (CD) site, a region that binds activators, inhibitors, and substrates. Little is known about the cellular consequences associated with this mutation, other than apparent increases in tumor resistance to pathway inhibitors. ERK2 E-K, like the mutation of the preceding aspartate (ERK2 D321N [D-N]) known as the sevenmaker mutation, causes increased activity in cells and evades inactivation by dual-specificity phosphatases. As opposed to findings in cancer cells, in developmental assays in *Drosophila*, only ERK2 D-N displays a significant gain of function, revealing mutation-specific phenotypes. The crystal structure of ERK2 D-N is indistinguishable from that of wild-type protein, yet this mutant displays increased thermal stability. In contrast, the crystal structure of ERK2 E-K reveals profound structural changes, including disorder in the CD site and exposure of the activation loop phosphorylation sites, which likely account for the decreased thermal stability of the protein. These contiguous mutations in the CD site of ERK2 are both required for docking interactions but lead to unpredictably different functional outcomes. Our results suggest that the CD site is in an energetically strained configuration, and this helps drive conformational changes at distal sites on ERK2 during docking interactions.

kinase | mutation | stability | ERK CD site

Extracellular signal-regulated kinase 2 (ERK2) is one of the most extensively studied enzymes in animal signal transduction (1–5). ERK2 is ubiquitously expressed, but remains inactive until 2 residues within its activation loop are dually phosphorylated by mitogen-activated protein kinase kinase (MEK), most commonly in response to extracellular growth factors that trigger the activity of highly conserved receptor tyrosine kinase signaling pathways. Active, doubly-phosphorylated ERK2 (ppERK2) has a broad spectrum of substrates, which allows it to control critical processes and functions in the organism, from the first cell divisions in embryos to learning and memory in adults (6–12). ERK2 activation is reversed by phosphatases, some of which are specific for ERKs and dephosphorylate the residues phosphorylated by MEK. Deregulated ERK2 activation has been associated with human diseases, including many types of cancer and a large class of developmental abnormalities (2, 13–16). Many of these diseases are caused by mutations that affect components of the signaling pathways leading to ERK2 activation, which makes these components common drug targets in oncology and other therapeutic areas. Detailed understanding of ERK2 activation mechanisms and their sensitivity to genetic and pharmacological perturbations will inform future therapeutic discovery. Our study addresses the effects of certain activating mutations in ERK2.

While studies of human diseases identified numerous pathogenic mutations in proteins involved in ERK2 activation, relatively few disease-related mutations have been reported in ERK2 itself (13). A notable exception is human ERK2 E322K (hERK2 E-K), identified in squamous cell carcinomas and identified as a cancer mutational hotspot; it is currently the most common mitogen-activated protein kinase 1 (MAPK1) missense mutation found in genomic data from tumors (17–19). The E-K mutation falls within the ERK2 common docking (CD) site, which is important for ERK2 binding to its regulators and substrates (20–22), and has been shown to enhance MEK-dependent ERK2 activation in an oral squamous cell carcinoma cell line (HSC6) (17). Studies with the *Drosophila* ERK2 ortholog, Rolled (referred to here as dERK), first demonstrated that mutations within the CD site can cause gain-of-function developmental phenotypes (23). In particular, the mutation analogous to hERK2 D321N (D-N) impairs dERK2 binding to phosphatases and results in increased ERK2 phosphorylation in response to extracellular growth factors (24). Here, we combine biochemical, genetic, and structural approaches

Significance

Extracellular signal-regulated kinases 1/2 (ERK1/2; mitogen-activated protein kinases) regulate physiological processes, including development and proliferation, and are overactive in many cancers. A conserved binding site docks effector proteins. Two adjacent negatively charged residues, one facing inward and the other into solvent, are required for docking, and have cancer-associated mutations. Mutation of the inward-facing residue disrupts ERK2 structure and decreases stability, while the outward-facing residue stabilizes the wild-type conformation. Both mutants cause similar changes in activities in vitro, yet drastically different *Drosophila* phenotypes, implying unanticipated functional differences. The clustered negative charges and stability differences suggest that the docking site is energetically strained by charge repulsion and provides energy to drive docking-induced conformational changes. Stability and energetic differences likely impact phenotypes.

Author contributions: M.H.C. initiated the project; C.A.T., K.W.C., S.Y.S., and M.H.C. designed research; C.A.T., K.W.C., S.E.K., S.E., S.S., and Y.-C.J. performed research; M.H.C. directed and interpreted certain experiments; C.A.T., K.W.C., S.E.K., S.E., S.S., C.W., J.W., and E.J.G. analyzed data; and C.A.T., S.E.K., S.Y.S., and M.H.C. wrote the paper.

Reviewers: A.M.B., Yale University School of Medicine; and P.S.S., University of Maryland School of Pharmacy.

The authors declare no conflict of interest.

Data deposition: The atomic coordinates and structure factors have been deposited in the Protein Data Bank, www.pdb.org (PDB ID codes 6OT6 [ERK2 D319N] and 6OTS [ERK2 E320K]).

[1]Present address: Lunenfeld-Tanenbaum Research Institute, Mount Sinai Hospital, Toronto, ON M5G 1X5, Canada.

[2]Present address: Early Discovery Pharmacology, Translational Medicine Research Centre, MRL, MSD, Singapore 138665.

[3]Present address: Computational Chemical Genomics Screening Center, Department of Pharmaceutical Sciences, University of Pittsburgh, Pittsburgh, PA 15206.

[4]To whom correspondence may be addressed. Email: melanie.cobb@utsouthwestern.edu.

This article contains supporting information online at www.pnas.org/lookup/suppl/doi:10.1073/pnas.1905015116/-/DCSupplemental.

Published online July 11, 2019.

to test whether the activating effects of ERK2 D-N and E-K have similar origins. Surprisingly, we found that while these 2 mutations are nearly indistinguishable when evaluated in several commonly used biochemical assays, they cause different effects in *Drosophila*. Furthermore, they lead to surprisingly different changes in the structure and stability of ERK2. Our results reveal functional divergence of activating mutations within a critical docking site of one of the most highly studied cell-signaling enzymes and pose questions important for understanding ERK2 signaling in health and disease.

Results

Activation of Phosphatase DUSP6 by ERK2 and Mutants and Their Inactivation by DUSP6 In Vitro. The ERK2 CD site interacts with docking (D)/kinase interaction motifs (KIMs) typically of the form R/K-R/K-$X_{3–5}$-φ-X-φ in substrates, regulators, and other interaction partners (21). All experiments were carried out with rat ERK2 (rERK2) D319N and E320K; rERK2 is 2 residues shorter than hERK2, lacking a glycine-alanine present at residues 8 and 9 of hERK2. We tested the interaction of rERK2 wild type and the CD site mutants D-N and E-K with a D/KIM-containing peptide corresponding to residues 712–728 from the ERK substrate RSK1. As expected, both rERK2 D-N and E-K failed to interact with the RSK1 peptide (Fig. 1*A*). Similarly, we found that the E-K mutation also disrupts the interaction with the D/KIM-containing dual-specificity phosphatase DUSP6 (MKP3) (*SI Appendix*, Fig. S1*A*). Because the D-N and E-K mutations in the CD site interfere with the interaction of rERK2 with DUSP6, we examined DUSP6 activity toward the rERK2 mutants. DUSP6 dephosphorylated ppERK2 D-N and E-K, monitored as loss of immunoreactive $pTyr^{185}$/$pThr^{183}$ ERK2, but more slowly than wild-type ppERK2 (24) (Fig. 1*B*). DUSP6 is also allosterically activated by binding ERK2 (25). To

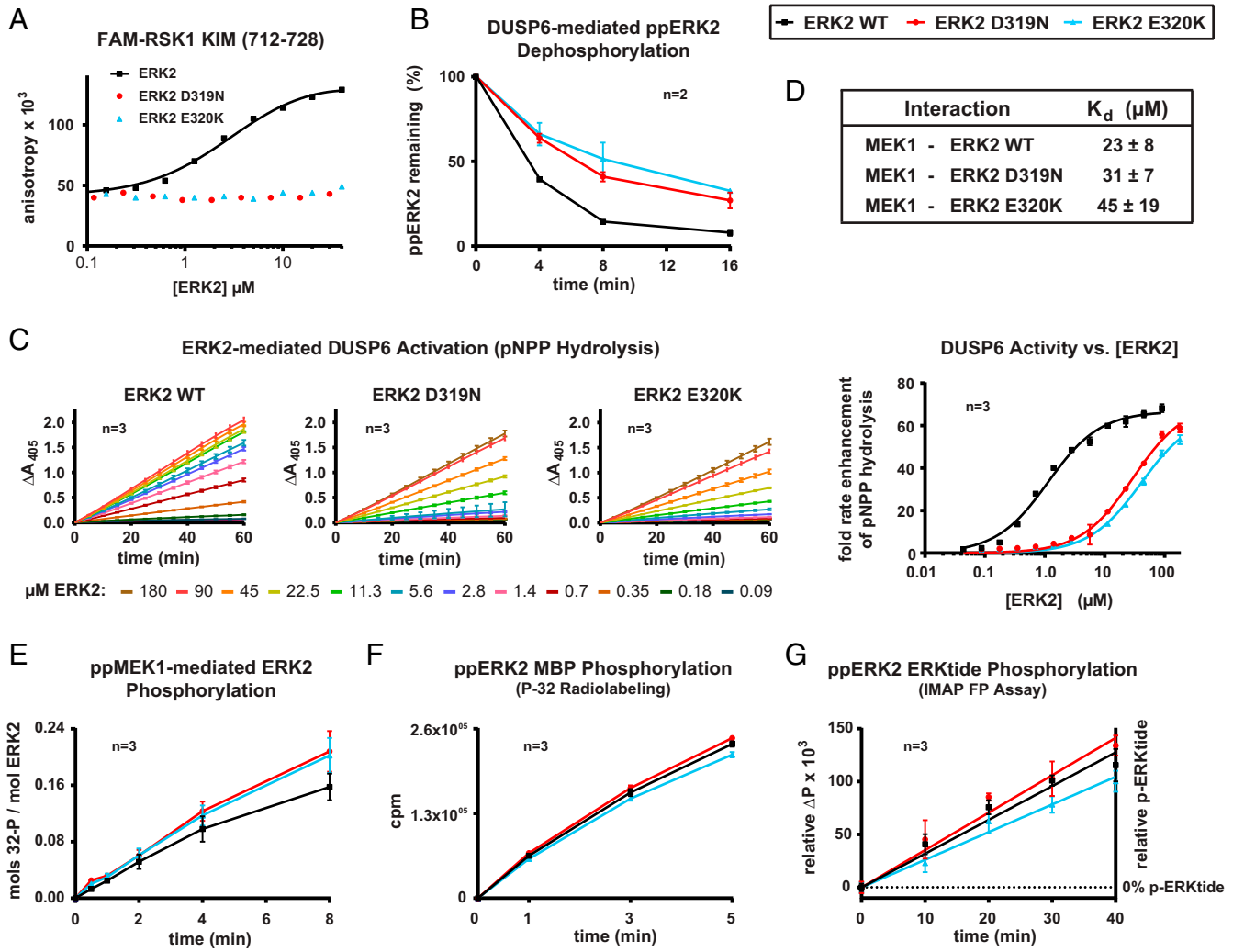

Fig. 1. ERK2 D-N and E-K mutations both disrupt DUSP6, but not MEK1, function in an in vitro setting. All panels show experiments with $n = 3$, except *B*. (*A*) Binding of RSK1 peptide (residues 712 to 728; 5-FAM-ahx-APQLKPIESSILAQRRVR-COO^-) to rERK2 wild type (black), D-N (rD319N, red), and E-K (rE320K, blue) as assessed by fluorescence polarization. ahx, 6-aminocaproic acid linker. (*B*) ppERK2 wild-type, D-N, and E-K dephosphorylation by DUSP6 as monitored by Western blot with ppERK2 antibody ($pTyr^{185}$/$pThr^{183}$). (*C*) rERK2 wild-type–, D-N–, and E-K–mediated activation of DUSP6 as monitored by p-nitrophenyl phosphate (pNPP) hydrolysis. (*Left*) Three panels indicate rates of pNPP hydrolysis (change in absorbance at 405 nm) as a function of time at various rERK2 concentrations. (*Right*) Summary is reaction rate enhancements (calculated from *Left*) as a function of rERK2 concentration. (*D*) Binding affinities of rERK2 wild type, D-N, and E-K to Cy5-labeled MEK1 as determined by microscale thermophoresis. K_d, dissociation constant. Refer to *SI Appendix*, Fig. S3*B*. (*E*) ppMEK1 phosphorylation of rERK2 wild type, D-N, and E-K as monitored by ^{32}P incorporation. (*F*) ppERK2 wild-type, D-N, and E-K phosphorylation of model substrate, MBP, as monitored by ^{32}P incorporation. cpm, counts per minute. (*G*) ppERK2 wild-type, D-N, and E-K phosphorylation of ERKtide-FAM (NH_3^+-IPTTPITTTYFFFK-5FAM-COO^-) as monitored by IMAP FP kinase assay.

determine effects of ERK2 mutations on allosteric activation of DUSP6, we monitored DUSP6 activity by p-nitrophenyl phosphate hydrolysis in the presence of unphosphorylated rERK2 wild type, D-N, and E-K. Unlike wild-type rERK2, which activated DUSP6 in the low micromolar range (apparent dissociation constant [K_d] = 1.1 ± 0.1 μM), both rERK2 D-N and E-K stimulated DUSP6 activity, but each required ~40-fold higher protein concentrations to achieve a similar level of DUSP6 activation (Fig. 1*C*). Unless in a scaffolded complex, these mutants would be unlikely to activate DUSP6 in vivo, because the concentrations of ERK2 mutants that would be required exceed a typical range in cells [<5 μM (26, 27)].

Activation and Activity of ERK2 E-K and D-N. MEK1 binds ERK2 through both the CD site and the MAPK insert region (21, 28–30). By microscale thermophoresis, a quantitative method to measure binding affinity using fluorophore-labeled MEK1, the MEK1 binding affinities of ERK2 wild-type, D-N, and E-K were similar at 23 ± 8, 31 ± 7, and 45 ± 19 μM, respectively (Fig. 1*D* and *SI Appendix*, Fig. S1*B*), suggesting that MAPK insert binding dominates in vitro interaction. Phosphorylated active MEK1 activates rERK2 wild type, D-N, and E-K with similar kinetics (Fig. 1*E*). Once phosphorylated, both ppERK2 D-N and E-K had kinase activity indistinguishable from wild type toward 2 different substrates (Fig. 1 *F* and *G*). Therefore, the mutations do not seem to affect MEK-dependent ERK2 activation or kinase activity in vitro.

In Vivo Evaluation of ERK2 E-K and D-N. We asked whether the ERK2 mutants, which performed similarly in biochemical assays, operated differently within the context of a living organism. The following in vivo assays examined 2 well-characterized ERK-dependent signaling events in *Drosophila*. The first occurs during oogenesis in the follicular epithelium to establish the dorsal-ventral axis of the future embryo. The second occurs 2 h post-fertilization at the poles of the embryo, specifying the terminal structures of the future larva. We overexpressed wild type and mutant forms of the *Drosophila* ERK ortholog, Rolled (dERK), in these 2 different tissues and examined their effects on dERK-dependent gene expression and morphological structures. We observed that dERK D-N and E-K have unpredictably different effects, in contrast to the similar behaviors of their rat homologs in biochemical assays.

The first of the analyzed signaling events occurs during egg development. The ligand Gurken is locally secreted from the dorsal-anterior cortex of the oocyte and activates the *Drosophila* epidermal growth factor receptor (EGFR), establishing a gradient of dERK activity in the overlying follicular epithelium (31, 32). As anticipated, the amount of ppERK detected by immunofluorescence was higher at the embryo poles (Fig. 2 *A* and *C*). The active signal from dERK D-N was similar to that of wild type (Fig. 2 *C*, *Right*), while the signal from dERK E-K was higher than that of wild type at the embryo poles (Fig. 2 *C*, *Center*). Due to communication between the follicle cells and the oocyte, this signal influences gene expression in the adjacent

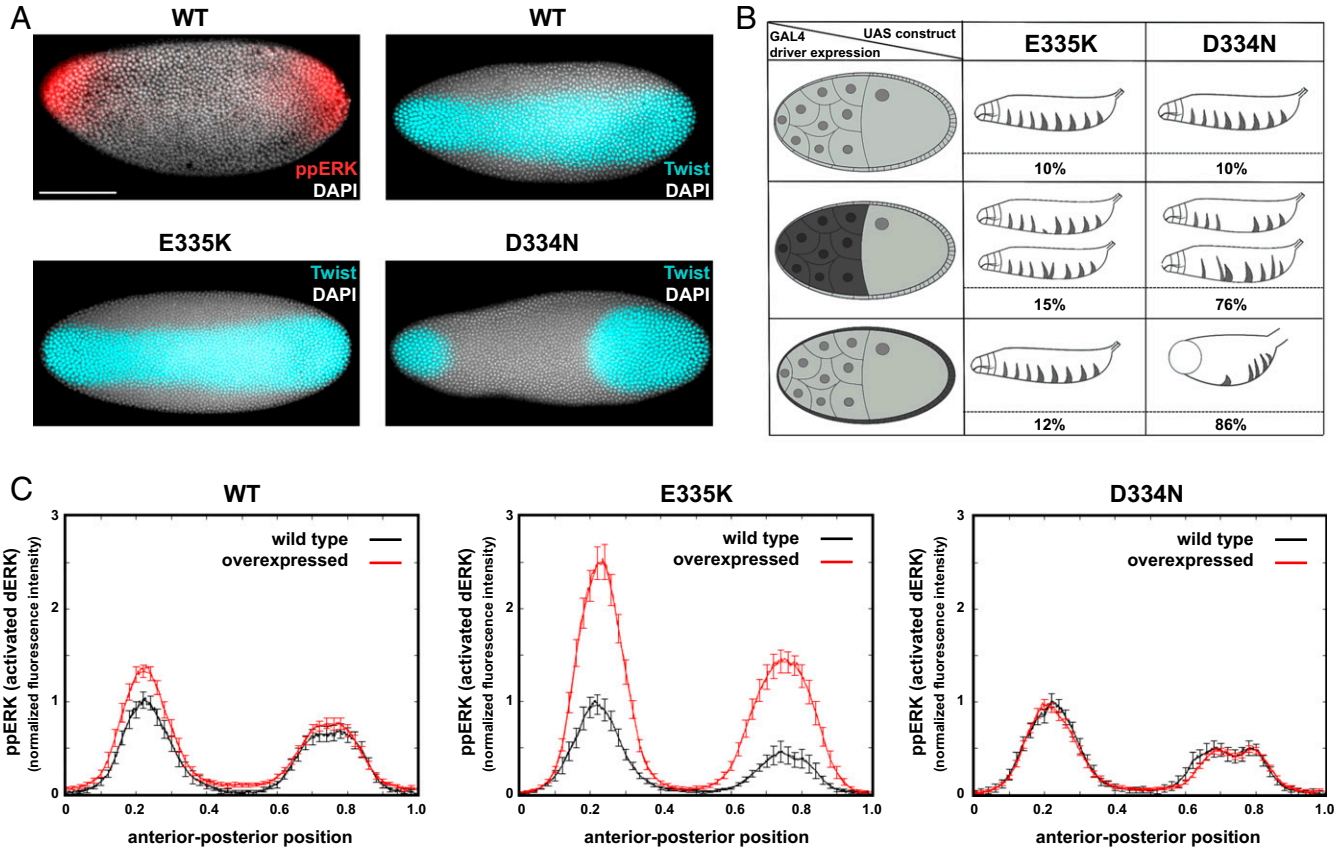

Fig. 2. Functional divergence of dERK mutants in *Drosophila*. Transgenic flies were created overexpressing the *Drosophila* ERK2 ortholog Rolled (dERK) wild type, D334N (D-N), and E335K (E-K). (*A*, *Top Left*) Lateral view of a typical wild-type (WT) embryo stained for ppERK. (*A*, *Top Right*) Ventral view of a typical WT embryo stained for Twist. (A, *Bottom*) Changes in Twist staining in the presence of dERK mutants (Scale bar, 100 μm). (*B*, *Top*) No mutant expression. Table summarizing percent lethality and observed phenotypes in dERK E-K and D-N in germline (*Middle*) and somatic tissue (*Bottom*). (*C*) dERK activation gradients in embryos. Plots of activated dERK (normalized ppERK fluorescence intensity) as a function of position in fly embryos are shown for both mutants and compared with wild type. About 60 embryos were used for each graph.

regions of the future embryo. A strong signal in dorsal follicle cells represses the gene *twi* (twist) on the dorsal side of the embryo. Accordingly, Twist is expressed on the ventral side of the embryo, where dERK activity in the follicular epithelium is low. We found that only dERK D-N disrupts dorsal-ventral embryonic patterning, based on the morphology of the embryonic cuticle and the expression of Twist (Fig. 2*A* and *SI Appendix*, Fig. S2). We observed a dramatic disruption in ventral expression of Twist only with dERK D-N, suggesting dERK activation in the lateral- and ventral-most parts of the follicular epithelium. These patterning defects caused severe disruptions of the embryonic exoskeleton and were associated with high embryonic lethality (Fig. 2*B* and *SI Appendix*, Fig. S2). Because the relative expression of the dERK proteins was similar, we conclude that dERK D-N and E-K have disparate effects on EGFR-dependent ERK signaling in the follicular epithelium.

The second signaling event occurs in the early embryo when a locally produced ligand of the receptor tyrosine kinase Torso, which is itself uniformly expressed, activates the dERK pathway at the terminal regions of the embryo. dERK signaling at the embryonic termini counteracts gene repression by the transcriptional repressor Capicua (Cic) (33–35). At the same time, the dERK pathway is kept inactive in the central regions of the embryo, where Cic is needed to repress multiple patterning genes. In the absence of dERK activation, 8 abdominal segments are formed, coordinated by gradients of transcription factors, including Cic (36, 37). Even a small increase in dERK activation in the middle of the embryo interferes with their formation (23). In the early embryo, expression of dERK D-N caused a range of defects in embryo segmentation, including fusions or deletions within abdominal segments, similar to those caused by expression of other activating components of the dERK pathway. This indicates strong gain-of-function activity. On the other hand, expression of dERK E-K caused only single fusions or deletions in the middle abdominal segment, indicative of a weak gain of function (Fig. 2*B*). As expected, these phenotypes were associated with differences in embryonic lethality.

Despite small phenotypic consequences, expression of E-K caused a marked increase in dERK phosphorylation at the poles, where endogenous dERK signaling is triggered by locally activated Torso (Fig. 2*C*). This observation is consistent with the proposed increased susceptibility of dERK E-K to activation. Importantly, this is not a result of overexpression, as overexpression of wild-type dERK showed no increase in activity at the poles (Fig. 2*C*). This assay was more difficult to perform on the dERK D-N mutant, as many embryos do not form proper blastoderms and the dERK signal could not be measured accurately. In sum, these assays reveal strong functional differences between the 2 dERK mutants in vivo. Consequently, we assessed how these 2 adjacent mutations in the CD site of rERK2 differentially alter the overall structure and stability of the molecule.

Structural Analysis of ERK2 D-N and E-K. To gain insight into molecular differences in the 2 mutants in *Drosophila*, we examined their structures. The relative abundance of the *MAPK1* missense somatic mutation yielding hERK2 E-K is ∼22- to 44-fold greater than the majority of somatic missense mutations (only 1 or 2 instances for most mutations) in a publicly available database containing the combined results of 200 cancer genomics studies [cBioPortal (38)] (Fig. 3 *A*, *Top*). While E-K is by far the most heavily enriched mutation in cancer, other residues are also enriched to varying extents. Four of the 6 ERK2 residues with the highest mutational frequency (Glu^{79}, Arg^{133}, Asp^{319}, and Glu^{320}) are within or directly adjacent to the acidic region of the CD site (Fig. 3 *A*, *Bottom*). The other 2 residues, Arg^{146} and Arg^{189}, are around the ERK2 active site. Curiously, all are charged residues.

The acidic part of the ERK2 L16 loop harbors both the D-N and E-K mutations and runs along the backside of the kinase contacting both the N- and C-terminal domains. The aspartate is a solvent-facing surface residue that directly contacts D/KIMs, while the glutamate does not directly interact with docking motifs and, instead, points into the core structure, participating in an unusual, buried hydrogen-bonding network (Fig. 3*B*).

We determined the crystal structures of rERK2 D-N and E-K (Table 1) and found that their overall structures align with other ERK2 structures (Fig. 3 *C* and *D* and *SI Appendix*, Fig. S3*A*). rERK2 E-K had more substantial structural deviation than D-N compared with other ERK2 structures (all C_α rmsd): ERK2 (1.82 Å, Protein Data Bank [PDB] ID code 4GSB), ppERK2 (1.83 Å, PDB ID code 2ERK), ERK2 D-N (1.80 Å), and ERK2 bound to phosphatase-derived peptides ERK2:hematopoietic protein tyrosine phosphatase (HePTP) D/KIM (1.38 Å, PDB ID code 2GPH) and ERK2:DUSP6 D/KIM (1.88 Å, chain A, PDB ID code 2FYS) (38–41). In ERK2 E-K, 8 residues (rat 318 to 325) encompassing E-K in the L16 loop/CD site (Fig. 3 *C–E* and *SI Appendix*, Fig. S3*D*) are disordered, disabling docking of proteins to the CD site (*SI Appendix*, Fig. S1*A*). On the other hand, the structure of rERK2 D-N, which neutralizes the negative charge of one of the residues that directly interacts with the basic region of docking motifs, is almost identical to wild-type ERK2 (all C_α rmsd = 0.54 Å) (Fig. 3 *C* and *D* and *SI Appendix*, Fig. S3*A*).

First shown for the MAPK p38, the CD site is allosterically coupled to the conformation of the MAPK activation loop (39). Three activation loop conformations of ERK2 (Fig. 3*G*) have been captured in crystal structures of unphosphorylated ERK2, ppERK2, and ERK2 bound to D/KIM peptides (40–42) (Fig. 3*G*). In the low-activity structure, the activating phosphorylation sites, rERK2 Tyr^{185} and Thr^{183}, are protected in pockets on the surface and the activation loop is tacked onto the MAPK insert. In the active structure, $pTyr^{185}$ and $pThr^{183}$ make distinct interactions on the protein surface to support greatly increased activity. In multiple docking motif-bound ERK2 structures, the activation loop is solvent exposed similar to p38 (39). The rERK2 E-K activation loop from Thr^{183} to Arg^{189}, including Tyr^{185} and Thr^{183}, assumes a solvent-exposed conformation virtually identical to that in peptide-bound structures (Fig. 3 *F* and *H* and *SI Appendix*, Fig. S3*E*). The rest of the rERK2 E-K activation loop is disordered and likely solvent-exposed as well (Fig. 3 *C*, *D*, and *H* and *SI Appendix*, Fig. S3*E*). This third conformation is energetically accessible in the absence of docking peptides in rERK2 E-K. Since the exposed activation loop conformation is observed in multiple structures, each with different crystal lattices, it is unlikely to be caused by crystal contacts. Thus, the ERK2 E-K mutation mimics the conformational changes induced by CD site engagement by docking motifs.

In addition, we attempted to seed rERK2 D-N crystals with rERK2 E-K crystals and rERK2 E-K crystals with rERK2 D-N and wild-type crystals, but neither was successful. However, we were able to seed rERK2 D-N crystals with rERK2 wild-type crystals, which suggests that the structure of rERK2 E-K is not compatible with the crystal lattice of the rERK2 wild-type and D-N crystals used in this study. Both the rERK2 D-N and E-K lattices are capable of supporting the solvent-exposed and buried activation loop conformations based on structural alignments, indicating that no steric clashes exist with the surrounding crystal lattice.

Effects of CD Site Mutations on ERK2 Stability. The solvent-exposed conformation of the rERK2 E-K activation loop decreases activation loop contacts with the MAPK insert (Fig. 3*F*). A second docking site, the F site, is made up of elements from the MAPK insert, helices αF and αG, and the ERK2 activation loop (28–30), and is required for interactions between phenylalanine-containing FxF motifs. The activation loop conformation modulates the affinity for FxF motifs. Electron density for the activation loop near the residues of the MAPK insert that make up part of the F site in the rERK2 E-K mutant is absent.

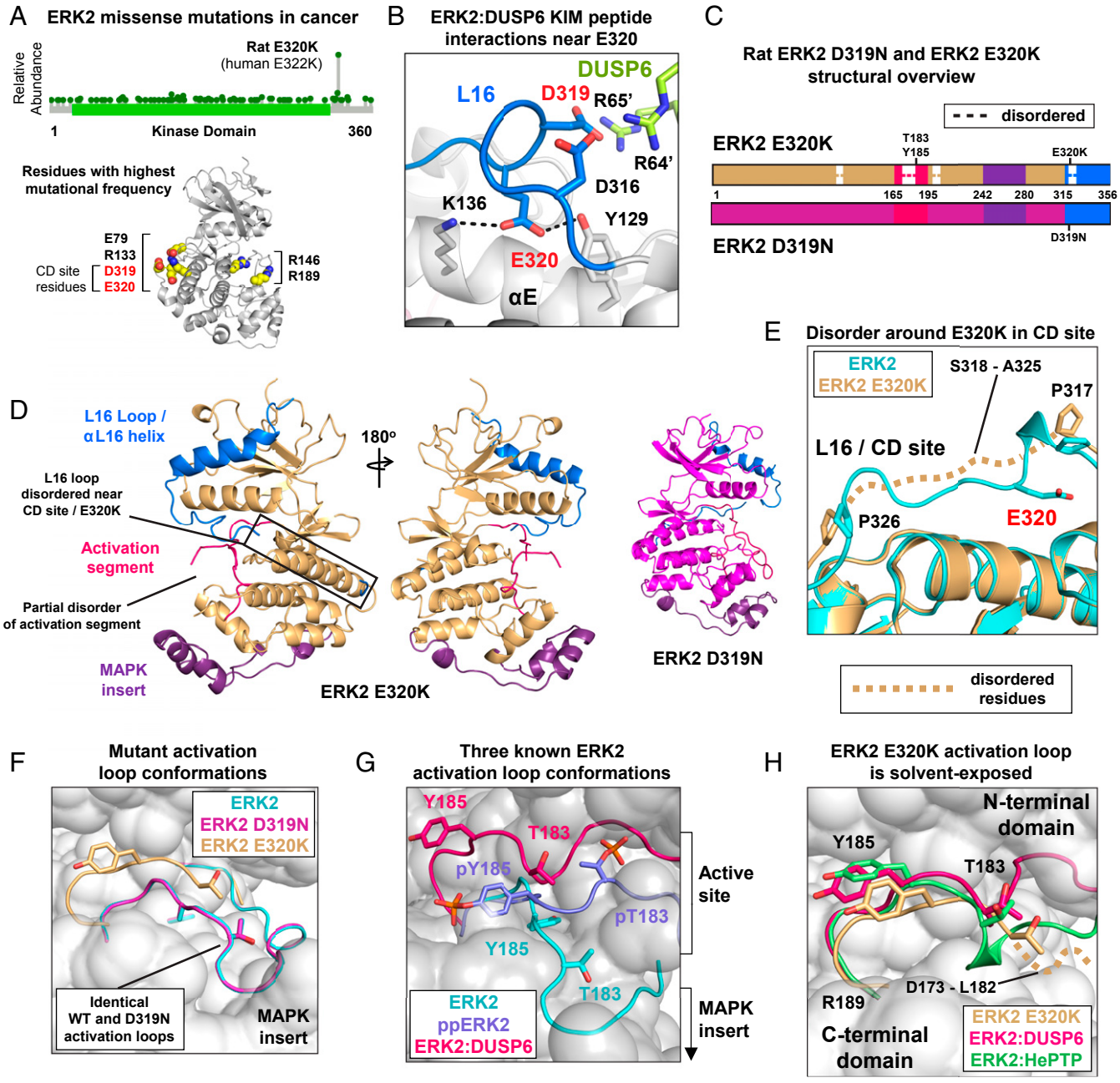

Fig. 3. Crystal structures of ERK2 CD site mutants D-N and E-K reveal areas of structural disruption and activation loop allosteric effects. (*A*, *Top*) Schematic of hERK2 with identified missense mutations in the *MAPK1* gene shown as green dots. Dots represent combined results of 200 large-scale cancer genomics studies found at cBioPortal (37). Dot height represents the relative abundance of the given mutation. hERK2 E322K (corresponding to rERK2 E320K) is the most abundant. (*A*, *Bottom*) Residues with the highest mutational frequencies (≥5 instances; rat numbering; Glu^{79} = 5, Arg^{133} = 8, Arg^{146} = 5, Arg^{189} = 6, Asp^{319} = 9, Glu^{320} = 44) are indicated in yellow on the crystal structure diagram of ERK2. Four of the 6 most highly mutated residues cluster near the CD site. (*B*) Close-up view of the interactions between the dual-arginine residues in the DUSP6 KIM peptide (lime) and the acidic residues Asp^{316}/Asp^{319} (red label) in the rERK2 L16 loop (blue) that makes up part of the CD site. Glu^{320} (red label) is a buried charge that points inward toward the kinase domain, and Asp^{319} points out into solvent. (*C*) Structural overview of rERK2 E-K (orange) and D-N (magenta). The schematic indicates positions of relevant structural elements and residues, and regions of disorder in the crystal structure (dashed lines). The activation loop (pink), MAPK insert (purple), and L16 loop and αL16 helix (blue) are shown. (*D*) Structures of rERK2 E-K (orange) and D-N (magenta). D-N is virtually identical to wild type, while E-K has disorder within the activation loop and L16 loop around the E-K mutation. *SI Appendix*, Fig. S3*A* shows structural alignments compared with wild type. (*E*) Comparison of the L16 loops (part of CD site) of inactive ERK2 (cyan) and rERK2 E-K (orange). The region around E-K (residues 318 to 325) is disordered in the crystal structure of rERK2 E-K. *SI Appendix*, Fig. S3*D* shows an electron density map. (*F*) Comparison of the activation loop conformations of rERK2 wild type (WT), D-N, and E-K. E-K is solvent-exposed, and D-N is identical to WT. *SI Appendix*, Fig. S3*E* shows electron density maps. (*G*) Three known conformations of the rERK2 activation loop around the activating phosphorylation sites Tyr^{185} and Thr^{183}: inactive ERK2 (PDB ID code 4GSB, cyan), active ppERK2 (light purple), and ERK2:DUSP6 KIM (pink). (*H*) Comparison of rERK2 E-K activation loop (orange) conformation near Tyr^{185}/Thr^{183} to structures of ERK2 bound to KIM peptides derived from DUSP6 (pink) and HePTP (green). (PDB ID codes: 4GSB [ERK2 WT], 2ERK [ppERK2], 6OT6 [ERK2 D319N], 6OTS [ERK2 E320K], 2FYS [ERK2:DUSP6], and 2GPH [ERK2:HePTP]).

Table 1. ERK2 mutant crystallographic data and refinement statistics

	ERK2 D319N	ERK2 E320K
Data collection		
Resolution, Å	50 to 1.65 (1.68 to 1.65)	50 to 2.1 (2.14 to 2.10)
Space group	$P2_1$	C2
Cell dimensions		
a, b, c; Å	48.9, 70.3, 60.5	182.3, 41.9, 50.3
α, β, γ; °	90, 109.6, 90	90, 105.9, 90
Unique reflections	45,537 (2,250)	19,252 (568)
Redundancy	7.4 (6.8)	4.0 (3.3)
Completeness, %	98.0 (96.4)	88.5 (53.1)
<I/σ(I)>	18.9 (1.9)	23.3 (1.7)
R_{merge}	0.107 (1.526)	0.055 (0.605)
R_{pim}	0.042 (0.610)	0.031 (0.357)
$CC_{1/2}$ (in highest resolution shell)	0.64	0.63
Refinement		
R_{work}/R_{free}, %	16.8/20.0	23.1/26.3
Bond rmsd	0.005	0.003
Angle rmsd	0.7	0.582
Ramachandran favored, %	98	91.4
Ramachandran outliers, %	0.3	0.3
<B-factor>	25.7	76.7
Rotamer outliers, %	1.2	3.4
Clashscore	3.2	3.7

rERK2 E-K helices αF and αG and MAPK insert helices have high B-factors indicative of increased mobility (Fig. 4 *A* and *B*). B-factors for the C-terminal domain of rERK2 E-K were overall higher relative to the N-terminal domain, in contrast to previous ERK2 structures (Fig. 4 *A* and *B* and *SI Appendix*, Fig. S3 *B* and *C*). The majority of intermolecular contacts with symmetry-related molecules in the crystal lattice are mediated by the N-terminal domain (*SI Appendix*, Fig. S3*C*). Interdomain motion is likely greater, because C-terminal domain B-factors increase as a function of distance from the kinase hinge despite the fact that E-K is ∼20 Å from the hinge (Fig. 4*A*). The B-factor relationship to the kinase hinge, and the fact that other D-KIM–bound ERK2 structures do not have similar properties as rERK2 E-K, imply that the increased B-factors are not the result of localized destabilization caused by loss of activation loop contacts. The increased interdomain mobility observed in the rERK2 E-K C-terminal domain is likely not apparent in the N-terminal domain because of the presence of considerably more crystal lattice contacts (*SI Appendix*, Fig. S3*C*).

rERK2 D-N and E-K both phosphorylated Ser^{383} of ELK1, an ERK2 substrate known to interact through the ERK2 F site (43), to similar extents (Fig. 4*A* and *SI Appendix*, Fig. S4*D*), and both mutants phosphorylated an FxF motif-containing peptide substrate (which binds the F site) similarly (Fig. 1*G*). These findings support the conclusion that the enhanced B-factors observed in ERK2 E-K are due to enhanced interdomain motion as opposed to localized destabilization around the F site.

To evaluate the impact of the increased disorder in rERK2 E-K, we measured effects of various mutations on thermal stability (Fig. 4*C*). rERK2 E-K is destabilized by almost 5 °C relative to wild-type rERK2, most likely as a consequence of introducing charge repulsion in the internal hydrogen bonding network (denoted by dotted lines in Fig. 3*B*). To evaluate the effect of another mutation that increases ERK2 flexibility and partially activates it, we introduced a smaller residue in place of the gatekeeper residue, Q103A, located in the kinase hinge (44). Mutation to Q103A also destabilizes rERK2 by nearly 5 °C (Fig. 4*C*). In contrast, rERK2 D-N was unexpectedly stabilized by almost 5 °C relative to wild type and nearly 10 °C relative to rERK2 E-K (Fig. 4*C*). Increased stability is likely due to eliminating a negative charge in the CD site charge cluster, $_{316}$DXXDE$_{320}$ (Fig. 3*B*). To provide perspective on the increased stability of rERK2 D-N, we mutated another negatively charged solvent-exposed residue on the surface of rERK2, E347Q. Mutation to E347Q, unlike D-N, had no effect on rERK2 stability (Fig. 4*C*). These results highlight the significance of the CD site as an energetic hot spot.

To control for potential sample heterogeneity due to autophosphorylation in our recombinant protein preparations, we utilized a purification scheme that removed ppERK2 (*SI Appendix*, Fig. S4*A*). In addition, we utilized dynamic light scattering to control for potential aggregation caused by the mutations. rERK2 wild type, D-N, and E-K all had nearly identical hydrodynamic radii, and aggregates were not detected (Fig. 4*D* and *SI Appendix*, Fig. S4*B*).

Discussion

One of the main challenges in understanding the functional consequences of mutations affecting cell signaling proteins is that each of them engages in multiple interactions, and because each of these interactions might be differentially affected by the same mutation, the overall phenotypes cannot be predicted by examining any single interaction or process. Our studies of the D-N and E-K mutations in the CD site of ERK2 underscore this complexity. We found that the effects of mutations are indistinguishable in vitro, based on the decreased rates of ERK2 dephosphorylation by DUSP, similar rates of ERK2 phosphorylation by MEK, and decreased ERK2-dependent activation of DUSP phosphatase activity. None of the quantitative changes observed in vitro could have predicted the strikingly different phenotypes caused by expression of the 2 dERK variants in *Drosophila*, where dERK D-N has significantly higher lethality, even though the E-K mutant displays greater signal-dependent phosphorylation.

The disparate effects of activating mutations in vivo prompted us to take a closer look at their effects on ERK2 itself and revealed that they result in dramatically different changes in the structure and stability of ERK2. The consequences of the 2 CD site mutations, one involving no conformational change and the other involving long-range conformational changes, highlight the

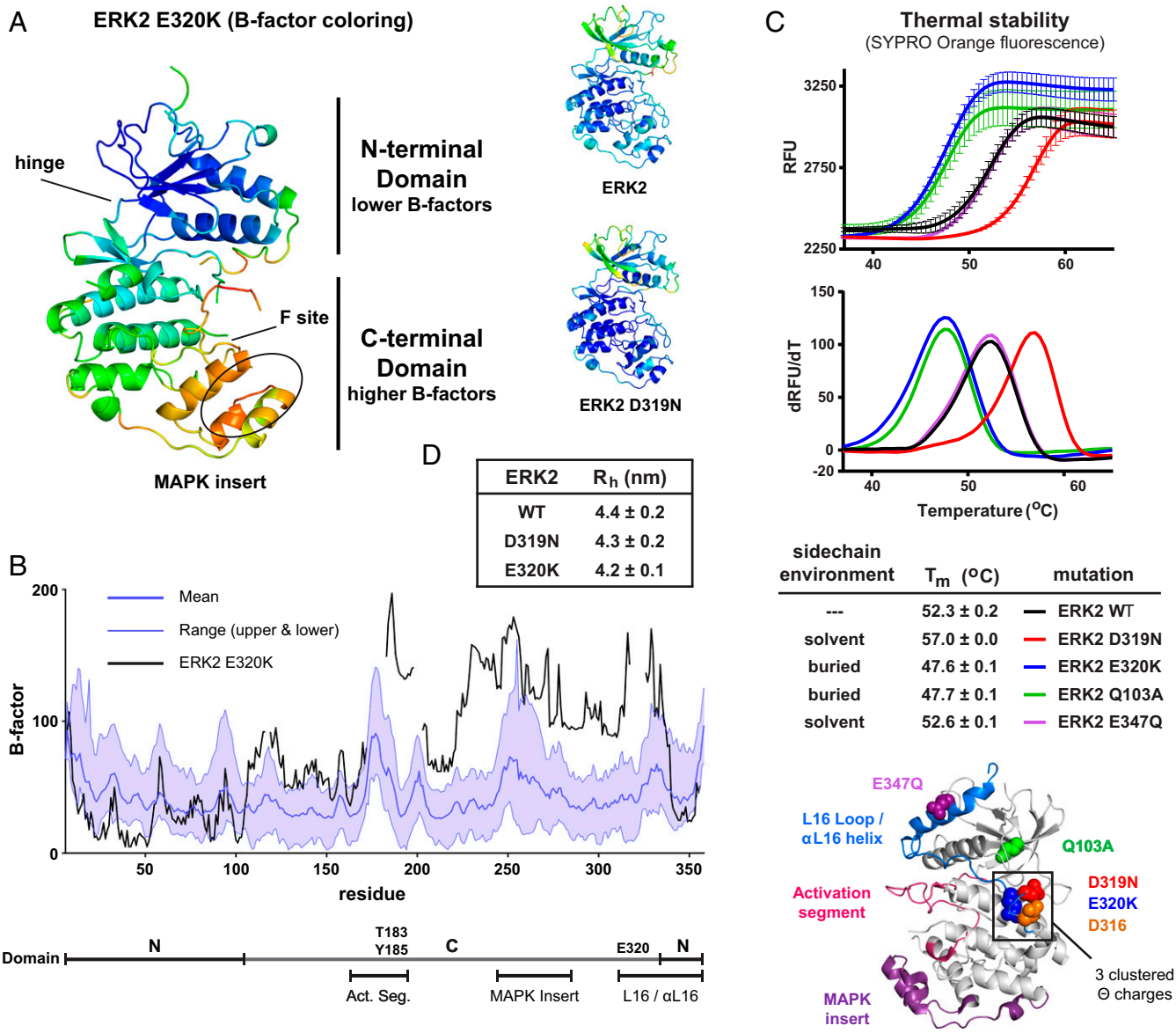

Fig. 4. E-K mutant destabilizes rERK2, and D-N mutant stabilizes rERK2. (*A* and *B*) Structures of rERK2 E-K, D-N, and wild type colored by B-factors and a B-factor plot comparing rERK2 E-K B-factors with those of 9 other ERK2 structures with similar resolutions (1.9 to 2.6 Å), but all different crystal lattices (PDB ID codes 2FYS, 2GPH, 3C9W, 3O71, 3TEI, 4H3P, 4NIF, 4XJ0, and 5BUE). The MAPK insert, F site (FxF motif interactions), and substrate binding pocket (Ser/Thr-Pro specificity) are indicated. (*C*) Thermal stabilities of rERK2 wild type (black), D-N (red), E-K (blue), Q103A (gatekeeper residue, green), and E347Q (purple) as determined by thermal shift assay (differential scanning fluorimetry). Plots show SYPRO orange fluorescence as a function of temperature (relative fluorescent units [RFU]) and as the derivative of the fluorescence as a function of temperature (dRFU/dT). The table indicates the denaturation midpoint (T_m) and solvent environment of the side chain ($n = 3$). The structure indicates the positions of all of the mutations. (*D*) Hydrodynamic radii (R_h) of rERK2 wild type (WT), D-N, and E-K as determined by dynamic light scattering. The full dataset in *SI Appendix*, Fig. S4*B* does not indicate the presence of aggregates in any of the samples ($n = 3$).

roles of the 3 crystallographically observed configurations of ERK2 in pathway control (39–42, 45–47). The 3 ERK2 configurations are most stable under different conditions: when unphosphorylated; when phosphorylated; and when docked and interacting with phosphatase, kinase, or substrate partners. Furthermore, docking induces activating conformational changes for DUSPs (48, 49). We suspect that the 3 configurations contribute to pathway specificity: DUSP binding increases accessibility of the phosphorylation sites for chemistry, and the DUSP is inactive until it sees an optimum activator. The ERK2 D-N mutant stabilizes the unphosphorylated configuration so that it transitions less well to the docked configuration, and thus probably does not change the shape of the DUSP. The ERK2 E-K mutant destabilizes the unphosphorylated configuration so that it adopts the docked configuration, but is then less able to induce DUSP conformational changes.

Crystal structures are snapshots of proteins that, in solution, occupy multiple conformations in dynamic equilibrium. By NMR, phosphorylation of ERK2 leads to synchronized dynamics throughout the molecule, thought to be mediated by the hinge between the 2 domains and to cause increased catalytic efficiency (50). Without phosphorylation, coupled dynamics in ERK2 are minimal. However, mutation of hinge residues leads to enhanced flexibility and mimics phosphorylation (50). Four of 6 of the most highly mutated ERK2 residues in cancer are clustered within or around the CD site acidic region. The proximity of these residues

to the hinge suggests that perturbations within the CD site through either ligand binding or mutation could have an impact on the hinge, and thus affect ERK2 interdomain motion (*SI Appendix*, Fig. S4*C*). A previous NMR study of ERK2 showed D/KIMs were associated with chemical shift perturbations in residues in the hinge (Gln^{103}), the acidic patch of the CD site, and residues physically in between (e.g., Glu^{79}, which is mutated in cancer as illustrated in Figs. 3 *A* and *B* and 4*A*) (51). These findings, together with the fact that CD site binding causes solvent exposure of the activation loop, suggest the hinge provides a link between the CD site and the activation loop. In contrast to findings with ERK2, in an NMR study of the related MAPK p38, peptide binding to the CD site and phosphorylation were both required to induce uniform exchange dynamics thought to be mediated by the hinge (52). Even though both ERK2 and p38 have different requirements for dynamics-driven activation, both display an allosteric coupling between the CD site and the activation loop.

The 5 °C destabilization of ERK2 E-K is a consequence of the charge repulsion introduced by this mutant that affects an internal hydrogen bond network. Introducing a smaller side chain in place of the gatekeeper glutamine (rQ103A) also caused a 5 °C destabilization, presumably due to an increase in flexibility of the hinge region and, like the CD site, communication with the activation loop (44). Perhaps more surprising is the 5 °C stabilization resulting from adding an amide to the surface aspartate in ERK2 D-N, an effect not caused by neutralizing an analogous surface charge elsewhere on the protein. The result is a nearly 10 °C difference in stability between the 2 CD site mutants, again pointing to the energetic control of ERK2 from the CD site. This stability difference reveals uncharacterized ERK2 properties essential to its biological activities. The enhanced thermal stability of D-N suggests that part of the mechanism for allosteric control of the activation loop by the CD site results from strain induced by 3 adjacent negative charges. Charge repulsion imparts additional energy to the system that helps drive changes in the activation loop conformation following engagement of the CD site aspartates by basic residues in D/KIMs. The relative stabilities of the ERK2 mutants present strong evidence that the CD site is an energetic hot spot in ERK2.

Going forward, it will be important to establish a mechanistic connection between this structural view of the effects of activating mutations provided by our study and their differential effects in vivo. We expect that critical insights will be provided by comparison of the global ERK2 interactomes. These studies may explain why the E-K mutant causes relatively minor developmental phenotypes in *Drosophila* and why it is much more commonly observed in sequencing studies of human cancers. While our results imply that other MEKs and DUSPs will behave similarly to MEK1 and DUSP6, additional studies analyzing the effects of the ERK2 mutations on activation and deactivation by other upstream kinases and phosphatases could yield mechanistic insights if differences in regulation are observed. Our results suggest that it will also be important to expand the scope of our biochemical, structural, and functional studies of ERK2 regulation and function to other ERK2 mutants, which might ultimately explain the dramatic differences between the functional impact of mutations in ERK2 and other components of the ERK2-dependent signaling networks.

Materials and Methods

Fluorescence Polarization. A total of 100 nM FAM-RSK1 712 to 728 (5FAM-ahx-APQLKPIESSILAQRRVR-COO^-) and varying concentrations of ERK2 were combined in 25 mM Tris·HCl (pH 7.75), 100 mM NaCl, and 1 mM dithiothreitol (DTT). Anisotropy was measured using a BioTek Synergy H1 multimode plate reader with a fluorescein isothiocyanate (FITC) fluorescence polarization (FP) filter cube. Data were fit with GraphPad Prism to a 1-site binding model.

Microscale Thermophoresis. Binding affinity measurements of ERK2 to cysteine-labeled (Cy5 dye) MEK1 were made on a NanoTemper Microscale Thermophoresis instrument. Samples were in 25 mM Tris·HCl (pH 7.6), 100 mM NaCl, 1 mM Tris(2-carboxyethyl)phosphine (TCEP), 1 mM ethylenediaminetetraacetic acid (EDTA), and 0.05% Tween. MEK1 was 50 nM. Data were analyzed using PALMIST software with a T-Jump model to account for effects of temperature-dependent protein destabilization (53).

Phosphatase Assays. Recombinant MKP-3 (0.14 μM; Enzo) was combined with 1 μM recombinant ppERK2 proteins in 10 mM Hepes (pH 8.0), 10 mM $MgCl_2$, 1 mM benzamidine, and 1 mM DTT, and was incubated for up to 16 min at room temperature. Aliquots were withdrawn at the indicated times and added to tubes containing 5× Laemmli sample buffer to terminate the reactions. Samples were immunoblotted using a ppERK antibody (Sigma). Changes in phosphorylation state were quantified using LiCor Odyssey infrared imaging.

p-Nitrophenyl Phosphate Hydrolysis Assays. Assays consisted of 100 mM Tris (pH 7.5), 100 mM NaCl, 0.5 mM TCEP, 1 mM EDTA, 20 mM p-nitrophenyl phosphate, 300 nM recombinant MKP3 tagged at the N terminus with maltose binding protein, and varying concentrations of ERK2 added to a 384-well plate. The production of p-nitrophenol was measured by absorbance at 405 nm using a BioTek Synergy H1 multimode plate reader.

Kinase Assays. To measure MEK1 kinase activity toward ERK2, 300 nM MEK1 and 3 μM ERK2 proteins were incubated in 10 mM Tris (pH 7.5), 10 mM $MgCl_2$, 50 μM adenosine 5′-triphosphate (ATP), and 0.01 mCi/μL [γ-32P]ATP at room temperature. A total of 5× Laemmli sample buffer was added, followed by heating for 5 min at 100 °C for analysis by denaturing gels. The ERK2 bands were excised from the gels after staining and analyzed by liquid scintillation counting in a Beckman LS6500 instrument. To measure ppERK2 kinase activity, reactions containing 1 mg/mL myelin basic protein (MBP) and 10 nM ppERK2 were incubated at 30 °C for varying amounts of time. Reactions were stopped by the addition of 5× Laemmli sample buffer, followed by heating for 5 min at 100 °C, for analysis on denaturing gels. MBP bands were excised from the gels and analyzed as above. To measure ppERK2 activity toward ERKtide-FAM ($NH3^+$-IPTTPITTTYFFF[K-5FAM]-COO^-) using the IMAP fluorescence polarization assay (IMAP FP Kit; Molecular Devices), 3 nM ppERK2 was incubated with 500 nM ERKtide-FAM for varying times in "IMAP FP reaction buffer with bovine serum albumin," 1 mM DTT, 50 μM ATP, and 15 mM $MgCl_2$. The reaction was stopped with binding buffer (60% buffer A, 40% buffer B, and 1:1,200 IMAP beads). Anisotropy was measured using a BioTek Synergy H1 multimode plate reader with an FITC FP filter cube.

Immunofluorescence. Assessments of ppERK in *Drosophila* were as described (54).

Fly Stocks. The E335K and D334N mutations were introduced into *Rolled* (gene coding for dERK) using site-directed mutagenesis with the Phusion enzyme and verified by sequencing. Mutant Rolled was then cloned into pTiger between the KpnI and NheI restriction sites. These constructs were integrated into the second chromosome using the ΦC31 integration system at the attP site in pTiger. These flies were crossed to 67;15 (a driver in the early embryo obtained from the laboratory of Eric Wieschaus, Princeton University) or TrafficJam-Gal4 flies to drive expression of mutant Rolled in the early embryo and follicle cells.

Lethality Counts. Embryos were collected from mutant flies crossed with 67;15 (as above) for 3 h (or until 100 to 200 embryos were laid). Embryos were left to develop at 25 °C for 30 h or longer. The total numbers of empty and unhatched eggshells were counted. Lethality was determined by comparing the number of unhatched embryos with total embryos laid. Around 1,000 total embryos were considered for both mutations.

Cuticle Preparation. Unhatched embryos were selected more than 24 h after embryo collection. Unhatched embryos were dechorionated for 1.5 min in bleach and incubated overnight at 65 °C in a 1:1 mixture of lactic acid and Hoyer's medium. Hatched larvae were selected more than 24 h after embryo collection. They were also incubated at 65 °C in a 1:1 mixture of lactic acid and Hoyer's medium. Embryos and larvae were imaged on a Nikon Eclipse Ni instrument.

X-Ray Crystallography. Crystals were obtained by hanging drop vapor diffusion. A total of 7 mg/mL ERK2 E320K in 25 mM Tris·Cl (pH 7.5), 100 mM NaCl,

1 mM EDTA, and 5 mM DTT was mixed with an equal volume of reservoir solution containing 28% (wt/vol) polyethylene glycol (PEG) 1500 and 100 mM Tris·Cl (pH 8.0). A total of 7.5 mg/mL ERK2 D319N in 25 mM Tris·Cl (pH 7.5), 100 mM NaCl, 1 mM EDTA, and 5 mM DTT was mixed with an equal volume of reservoir solution containing 1.5 M ammonium sulfate, 100 mM Hepes (pH 7.75), and 2% (vol/vol) PEG 500 monomethyl ether. D319N crystals were initially small needle clusters, but after 3 rounds of serial seeding, large plate crystals were obtained. Crystals were incubated at 20 °C and harvested at 1 wk for E320K and at 3 d for D319N. Diffraction data were collected at beamline 19-ID at the Advanced Photon Source (Argonne National Laboratory, Argonne, IL). Data were indexed, integrated, and scaled in HKL3000 (55). The structure of ERK2 E320K was determined using molecular replacement in PHASER in Phenix (56–58). The N- and C-terminal domains (residues 6 to 169 and 170 to 358) of the active ERK2 structure (PDB ID code 2ERK) were used as search models, and a similar procedure using ERK2 wild type (PDB ID code 4GBS) was employed for ERK2 D319N. The structures contain 1 molecule per asymmetric unit. Iterative rounds of refinement (TLS, rigid body, individual atomic displacement parameters, and atomic positions [only N-terminal domain atomic positions for E320K]) were carried out in phenix.refine, and model building was carried out in Coot (58–60). Secondary structure restraints were used early in model building for E320K. Simulated annealing was used early in model building for D319N. Model validation was conducted in phenix.refine, which uses analyses derived, in part, from the MolProbity web server (58, 60, 61).

Dynamic Light Scattering. ERK2 dynamic light scattering measurements were made using a DynaPro NanoStar (Wyatt Technologies). Samples purified by Superdex200 gel filtration at 24 μM (1 mg/mL) in 25 mM Tris·HCl (pH 7.6), 100 mM NaCl, 1 mM TCEP, and 1 mM EDTA were used. Analysis was carried out using the DYNAMICS software package.

Thermal Stability. Temperature-dependent changes in SYPRO orange fluorescence were monitored using a C1000 Thermal Cycler combined with a CFX96 Real-Time Monitoring System (Bio-Rad). ERK2 protein was at 5 μM in 25 mM Tris·HCl (pH 7.6), 100 mM NaCl, 1 mM TCEP, and 1 mM EDTA. T_m was defined as the temperature of maximum change in SYPRO orange fluorescence and determined in Microsoft Excel.

Protein Expression and Purification. His_6-tagged rat ERK2 wild type and mutants in a NpT7 vector were expressed in *Escherichia coli* DE3. Fifty-milliliter starter cultures were grown overnight at 30 °C in the presence of 100 μg/mL ampicillin in Luria broth. Twenty milliliters was then used to inoculate 1-L cultures, which were grown at 30 °C. Protein expression was induced with 400 μM isopropyl-β-D-1-thiogalactopyranoside at an optical density at 600 nm = 0.7, and cultures were allowed to grow overnight at 30 °C (21 h postinduction worked best). Cultures were centrifuged, and pellets were frozen in liquid nitrogen. Pellets were thawed and resuspended in 50 mM Na-phosphate (pH 8.0) and 300 mM NaCl. Ten percent saturated lysozyme solution and 0.5% Triton-X were added, followed by sonication. Clarified lysates were incubated with nickel-nitrilotriacetic acid beads (0.5 mL of beads per liter of culture) for 1 h at 4 °C while rocking. All subsequent washes were carried out in a conical tube, and beads were sedimented by centrifugation. Beads were washed 5 times each with 10 bed volumes of 50 mM Na-phosphate, 300 mM NaCl, and 40 mM imidazole (pH 8.0). Proteins were eluted by incubation with 3 bed volumes of 50 mM Na-phosphate (pH 8.0), 300 mM NaCl, and 300 mM imidazole (pH-adjusted) for 30 min at 4 °C with occasional stirring by pipette. Before MonoQ purification, the sample was filtered through a 0.2-μm filter and then dialyzed into 10 mM Tris·HCl (pH 8.2) and 0.5 mM TCEP (buffer A). Filtering is essential to prevent aggregation during dialysis into the low-salt buffer. Samples were passed over a MonoQ GL 5/5 column (GE Life Sciences) at 0.3 $mL{\cdot}min^{-1}$. Protein was eluted by 3 column volumes of buffer A, followed by a 0 to 25% gradient of buffer B (buffer A + 1 M NaCl) over 40 volumes. Western blotting using ppERK2 antibody was used to determine which fractions to exclude due to autophosphorylation. Protein is highly pure after MonoQ, but Superdex200 gel filtration was used to prepare protein for biophysical measurements and crystallography. Gel filtration buffer was 25 mM Tris·HCl (pH 7.6), 100 mM NaCl, 1 mM TCEP, and 1 mM EDTA.

Data and Materials Availability. The following crystallographic datasets were used: ERK2 D319N (PDB ID code 6OT6) and ERK2 E320K (PDB ID code 6OTS). All other materials are available upon request.

ACKNOWLEDGMENTS. We thank Dominika Borek, Diana Tomchick, and Zhe Chen (Department of Biophysics, UT Southwestern) for advice and assistance with crystallization, data collection, and data processing; Chad Brautigam and Shih-Chia Tso (Department of Biophysics, UT Southwestern) for assistance with dynamic light scattering and microscale thermophoresis; Radha Akella (Department of Biophysics, UT Southwestern) for assistance with thermal stability assays; Dean Smith and Ben Weaver (Department of Pharmacology, UT Southwestern) for thoughtful comments on the manuscript; Michael Reese (Department of Pharmacology, UT Southwestern) for suggestions about plotting B-factor data; Aroon Karra, Wen-Huang Ko, Jihan Osborne, and other current and former members of the M.H.C. laboratory for their advice and assistance with specific aspects of this project; and Dionne Ware for administrative assistance. Results shown in this report are derived from work performed at the Argonne National Laboratory, Structural Biology Center at the Advanced Photon Source. The Argonne National Laboratory is operated by the University of Chicago Argonne, LLC, for the US Department of Energy, Office of Biological and Environmental Research, under contract DE-AC02-06CH11357. This project was supported by Welch Foundation Grants I1243 (to M.H.C.) and I1128 (to E.J.G.) and by NIH Grants R37DK34128 (to M.H.C.) and R01GM086537 (to S.Y.S.). C.A.T. was supported in the late stages of this work by Cancer Prevention and Research Institute of Texas Training Grant RP160157. Additional support was provided by National Cancer Institute Grant P30CA142543 to the Harold C. Simmons Comprehensive Cancer Center for core facilities.

1. T. Kunath *et al.*, FGF stimulation of the Erk1/2 signalling cascade triggers transition of pluripotent embryonic stem cells from self-renewal to lineage commitment. *Development* **134**, 2895–2902 (2007).
2. G. Chan, S. Gu, B. G. Neel, Erk1 and Erk2 are required for maintenance of hematopoietic stem cells and adult hematopoiesis. *Blood* **121**, 3594–3598 (2013).
3. H. Ryu *et al.*, Frequency modulation of ERK activation dynamics rewires cell fate. *Mol. Syst. Biol.* **11**, 838 (2015).
4. R. Buscà *et al.*, ERK1 and ERK2 present functional redundancy in tetrapods despite higher evolution rate of ERK1. *BMC Evol. Biol.* **15**, 179 (2015).
5. M. Raman, W. Chen, M. H. Cobb, Differential regulation and properties of MAPKs. *Oncogene* **26**, 3100–3112 (2007).
6. T. S. Lewis *et al.*, Identification of novel MAP kinase pathway signaling targets by functional proteomics and mass spectrometry. *Mol. Cell* **6**, 1343–1354 (2000).
7. H. Kosako *et al.*, Phosphoproteomics reveals new ERK MAP kinase targets and links ERK to nucleoporin-mediated nuclear transport. *Nat. Struct. Mol. Biol.* **16**, 1026–1035 (2009).
8. S. M. Carlson *et al.*, Large-scale discovery of ERK2 substrates identifies ERK-mediated transcriptional regulation by ETV3. *Sci. Signal.* **4**, rs11 (2011).
9. M. Courcelles *et al.*, Phosphoproteome dynamics reveal novel ERK1/2 MAP kinase substrates with broad spectrum of functions. *Mol. Syst. Biol.* **9**, 669 (2013).
10. S. A. Stuart *et al.*, A phosphoproteomic comparison of B-RAFV600E and MKK1/2 inhibitors in melanoma cells. *Mol. Cell. Proteomics* **14**, 1599–1615 (2015).
11. S. Meloche, J. Pouysségur, The ERK1/2 mitogen-activated protein kinase pathway as a master regulator of the G1- to S-phase transition. *Oncogene* **26**, 3227–3239 (2007).
12. I. S. Samuels *et al.*, Deletion of ERK2 mitogen-activated protein kinase identifies its key roles in cortical neurogenesis and cognitive function. *J. Neurosci.* **28**, 6983–6995 (2008).
13. P. T. Wan *et al.*; Cancer Genome Project, Mechanism of activation of the RAF-ERK signaling pathway by oncogenic mutations of B-RAF. *Cell* **116**, 855–867 (2004).
14. K. A. Rauen *et al.*, Proceedings from the 2009 genetic syndromes of the Ras/MAPK pathway: From bedside to bench and back. *Am. J. Med. Genet. A.* **152A**, 4–24 (2010).
15. A. G. Stephen, D. Esposito, R. K. Bagni, F. McCormick, Dragging ras back in the ring. *Cancer Cell* **25**, 272–281 (2014).
16. R. Sever, J. S. Brugge, Signal transduction in cancer. *Cold Spring Harb. Perspect. Med.* **5**, a006098 (2015).
17. R. Arvind *et al.*, A mutation in the common docking domain of ERK2 in a human cancer cell line, which was associated with its constitutive phosphorylation. *Int. J. Oncol.* **27**, 1499–1504 (2005).
18. M. Mahalingam *et al.*, ERK2 CD domain mutation from a human cancer cell line enhanced anchorage-independent cell growth and abnormality in Drosophila. *Oncol. Rep.* **20**, 957–962 (2008).
19. A. I. Ojesina *et al.*, Landscape of genomic alterations in cervical carcinomas. *Nature* **506**, 371–375 (2014).
20. S. H. Yang, P. R. Yates, A. J. Whitmarsh, R. J. Davis, A. D. Sharrocks, The Elk-1 ETS-domain transcription factor contains a mitogen-activated protein kinase targeting motif. *Mol. Cell. Biol.* **18**, 710–720 (1998).
21. T. Tanoue, M. Adachi, T. Moriguchi, E. Nishida, A conserved docking motif in MAP kinases common to substrates, activators and regulators. *Nat. Cell Biol.* **2**, 110–116 (2000).
22. D. Jacobs, G. J. Beitel, S. G. Clark, H. R. Horvitz, K. Kornfeld, Gain-of-function mutations in the *Caenorhabditis elegans* lin-1 ETS gene identify a C-terminal regulatory domain phosphorylated by ERK MAP kinase. *Genetics* **149**, 1809–1822 (1998).
23. D. Brunner *et al.*, A gain-of-function mutation in Drosophila MAP kinase activates multiple receptor tyrosine kinase signaling pathways. *Cell* **76**, 875–888 (1994).
24. C. M. Bott, S. G. Thorneycroft, C. J. Marshall, The sevenmaker gain-of-function mutation in p42 MAP kinase leads to enhanced signalling and reduced sensitivity to dual specificity phosphatase action. *FEBS Lett.* **352**, 201–205 (1994).

25. M. Camps *et al*., Catalytic activation of the phosphatase MKP-3 by ERK2 mitogen-activated protein kinase. *Science* **280**, 1262–1265 (1998).
26. J. Basken *et al*., Specificity of phosphorylation responses to MAP kinase pathway inhibitors in melanoma cells. *Mol. Cell. Proteomics* **17**, 550–564 (2018).
27. D. Romano *et al*., Protein interaction switches coordinate Raf-1 and MST2/Hippo signalling. *Nat. Cell Biol.* **16**, 673–684 (2014).
28. F. L. Robinson, A. W. Whitehurst, M. Raman, M. H. Cobb, Identification of novel point mutations in ERK2 that selectively disrupt binding to MEK1. *J. Biol. Chem.* **277**, 14844–14852 (2002).
29. D. Jacobs, D. Glossip, H. Xing, A. J. Muslin, K. Kornfeld, Multiple docking sites on substrate proteins form a modular system that mediates recognition by ERK MAP kinase. *Genes Dev.* **13**, 163–175 (1999).
30. T. Lee *et al*., Docking motif interactions in MAP kinases revealed by hydrogen exchange mass spectrometry. *Mol. Cell* **14**, 43–55 (2004).
31. L. A. Goentoro *et al*., Quantifying the Gurken morphogen gradient in Drosophila oogenesis. *Dev. Cell* **11**, 263–272 (2006).
32. J. J. Zartman *et al*., Pattern formation by a moving morphogen source. *Phys. Biol.* **8**, 045003 (2011).
33. R. Sopko, N. Perrimon, Receptor tyrosine kinases in Drosophila development. *Cold Spring Harb. Perspect. Biol.* **5**, a009050 (2013).
34. O. Grimm *et al*., Torso RTK controls Capicua degradation by changing its subcellular localization. *Development* **139**, 3962–3968 (2012).
35. G. Jiménez, S. Y. Shvartsman, Z. Paroush, The Capicua repressor–A general sensor of RTK signaling in development and disease. *J. Cell Sci.* **125**, 1383–1391 (2012).
36. J. Zeitlinger *et al*., Whole-genome ChIP-chip analysis of Dorsal, Twist, and Snail suggests integration of diverse patterning processes in the Drosophila embryo. *Genes Dev.* **21**, 385–390 (2007).
37. Y. Kim *et al*., Gene regulation by MAPK substrate competition. *Dev. Cell* **20**, 880–887 (2011).
38. E. Cerami *et al*., The cBio cancer genomics portal: An open platform for exploring multidimensional cancer genomics data. *Cancer Discov.* **2**, 401–404 (2012).
39. C. I. Chang, B. E. Xu, R. Akella, M. H. Cobb, E. J. Goldsmith, Crystal structures of MAP kinase p38 complexed to the docking sites on its nuclear substrate MEF2A and activator MKK3b. *Mol. Cell* **9**, 1241–1249 (2002).
40. F. Zhang, A. Strand, D. Robbins, M. H. Cobb, E. J. Goldsmith, Atomic structure of the MAP kinase ERK2 at 2.3 A resolution. *Nature* **367**, 704–711 (1994).
41. B. J. Canagarajah, A. Khokhlatchev, M. H. Cobb, E. J. Goldsmith, Activation mechanism of the MAP kinase ERK2 by dual phosphorylation. *Cell* **90**, 859–869 (1997).
42. T. Zhou, L. Sun, J. Humphreys, E. J. Goldsmith, Docking interactions induce exposure of activation loop in the MAP kinase ERK2. *Structure* **14**, 1011–1019 (2006).
43. K. A. Burkhard, F. Chen, P. Shapiro, Quantitative analysis of ERK2 interactions with substrate proteins: Roles for kinase docking domains and activity in determining binding affinity. *J. Biol. Chem.* **286**, 2477–2485 (2011).
44. M. A. Emrick *et al*., The gatekeeper residue controls autoactivation of ERK2 via a pathway of intramolecular connectivity. *Proc. Natl. Acad. Sci. U.S.A.* **103**, 18101–18106 (2006).
45. R. Akella, X. Min, Q. Wu, K. H. Gardner, E. J. Goldsmith, The third conformation of p38α MAP kinase observed in phosphorylated p38α and in solution. *Structure* **18**, 1571–1578 (2010).
46. Y. S. Heo *et al*., Structural basis for the selective inhibition of JNK1 by the scaffolding protein JIP1 and SP600125. *EMBO J.* **23**, 2185–2195 (2004).
47. S. Liu, J. P. Sun, B. Zhou, Z. Y. Zhang, Structural basis of docking interactions between ERK2 and MAP kinase phosphatase 3. *Proc. Natl. Acad. Sci. U.S.A.* **103**, 5326–5331 (2006).
48. M. Muda *et al*., The dual specificity phosphatases M3/6 and MKP-3 are highly selective for inactivation of distinct mitogen-activated protein kinases. *J. Biol. Chem.* **271**, 27205–27208 (1996).
49. Y. Y. Zhang, J. W. Wu, Z. X. Wang, A distinct interaction mode revealed by the crystal structure of the kinase p38α with the MAPK binding domain of the phosphatase MKP5. *Sci. Signal.* **4**, ra88 (2011).
50. Y. Xiao *et al*., Phosphorylation releases constraints to domain motion in ERK2. *Proc. Natl. Acad. Sci. U.S.A.* **111**, 2506–2511 (2014).
51. A. Piserchio *et al*., Solution NMR insights into docking interactions involving inactive ERK2. *Biochemistry* **50**, 3660–3672 (2011).
52. G. S. Kumar *et al*., Dynamic activation and regulation of the mitogen-activated protein kinase p38. *Proc. Natl. Acad. Sci. U.S.A.* **115**, 4655–4660 (2018).
53. T. H. Scheuermann, S. B. Padrick, K. H. Gardner, C. A. Brautigam, On the acquisition and analysis of microscale thermophoresis data. *Anal. Biochem.* **496**, 79–93 (2016).
54. B. Lim *et al*., Dynamics of inductive ERK signaling in the Drosophila embryo. *Curr. Biol.* **25**, 1784–1790 (2015).
55. Z. Otwinowski, W. Minor, "Processing of X-ray diffraction data collected in oscillation mode" in *Macromolecular Crystallography, Part A*, C. W. Carter, R. M. Sweet, Eds. (Academic Press, New York, 1997), pp. 307–326.
56. A. J. McCoy *et al*., Phaser crystallographic software. *J. Appl. Cryst.* **40**, 658–674 (2007).
57. A. J. McCoy, R. W. Grosse-Kunstleve, L. C. Storoni, R. J. Read, Likelihood-enhanced fast translation functions. *Acta Crystallogr. D Biol. Crystallogr.* **61**, 458–464 (2005).
58. P. D. Adams *et al*., PHENIX: A comprehensive python-based system for macromolecular structure solution. *Acta Crystallogr. D Biol. Crystallogr.* **66**, 213–221 (2010).
59. P. Emsley, K. Cowtan, Coot: Model-building tools for molecular graphics. *Acta Crystallogr. D Biol. Crystallogr.* **60**, 2126–2132 (2004).
60. P. V. Afonine *et al*., Towards automated crystallographic structure refinement with phenix.refine. *Acta Crystallogr. D Biol. Crystallogr.* **68**, 352–367 (2012).
61. I. W. Davis, L. W. Murray, J. S. Richardson, D. C. Richardson, MOLPROBITY: Structure validation and all-atom contact analysis for nucleic acids and their complexes. *Nucleic Acids Res.* **32**, W615–W619 (2004).